Calorimetrically determined U(VI) toxicity in Brassica napus correlates with oxidoreductase activity and U(VI) speciation

Sachs, S.; Geipel, G.; Bok, F.; Oertel, J.; Fahmy, K.;

Originally published:

August 2017

Environmental Science & Technology 51(2017)18, 10843-10849

DOI: https://doi.org/10.1021/acs.est.7b02564

Article

Calorimetrically determined U(VI) toxicity in Brassica napus correlates with oxidoreductase activity and U(VI) speciation

Susanne Sachs, Gerhard Geipel, Frank Bok, Jana Oertel, and Karim Fahmy

Environ. Sci. Technol., **Just Accepted Manuscript** • DOI: 10.1021/acs.est.7b02564 • Publication Date (Web): 25 Aug 2017

Calorimetrically determined U(VI) toxicity in *Brassica napus* correlates with oxidoreductase activity and U(VI) speciation

Susanne Sachs*, Gerhard Geipel, Frank Bok, Jana Oertel*, Karim Fahmy*

Helmholtz-Zentrum Dresden - Rossendorf, Institute of Resource Ecology,
Bautzner Landstraße 400, 01328 Dresden, Germany

*corresponding author
k.fahmy@hzdr.de

ABSTRACT

Radioecological studies depend on the quantitative toxicity assessment of environmental radionuclides. At low dose exposure, the life span of affected organisms is barely shortened enabling the transfer of radionuclides through an almost intact food chain. Lethality-based toxicity estimates are not adequate in this regime because they require higher concentrations. However, increased radionuclide concentration alters its speciation, rendering the extrapolation to the low dose exposure chemically inconsistent. Here, we demonstrate that microcalorimetry provides a sensitive real-time monitor of toxicity of uranium (in the U(VI) oxidation state) in a plant cell model of *Brassica napus*. We introduce the calorimetric descriptor "metabolic capacity" and show that it correlates with enzymatically determined cell viability. It is independent of physiological models and robust against the naturally occurring fluctuations in the metabolic response to U(VI) of plant cell cultures. In combination with time-resolved laser-induced fluorescence spectroscopy and thermodynamic modeling, we show that the plant cell metabolism is affected predominantly by hydroxo-species of U(VI) with an IC_{50} threshold of ~90 µM. The data emphasize the yet little exploited potential of microcalorimetry for the speciation-sensitive ecotoxicology of radionuclides.

Keywords

Uranium, plant cells, metabolism, isothermal microcalorimetry, speciation, TRLFS, thermodynamic modeling

INTRODUCTION

The transfer of environmental radionuclides into the food chain is a central concern in the safety assessment of both nuclear waste repositories and remediation strategies in radioactively contaminated areas. The interaction of radionuclides with plants is mostly described by transfer factors without knowledge of underlying mechanisms. However, recent studies of the interaction of radionuclides, e.g., uranium, with plants revealed the importance of radionuclide speciation. The latter was correlated with uranium uptake from nutrient medium and translocation in plants.[1] Cross-species studies showed that both processes are speciation-dependent[2,3] and uranium toxicity can be further modulated by phosphate.[4] In addition to speciation effects on uranium uptake and oxidative stress response,[5,6] the redox state of uranium and the intracellular glutathione pool have also been investigated in plants.[7] The *in situ* speciation of uranium in plants[8] and their subcellular compartments[9] has been observed by spectroscopy. In response to heavy metal stress, plants synthesize protective metal-binding metabolites, store metal chelates in the vacuole or secrete them into the rhizosphere.[10] This reduces metal toxicity which originates in the replacement of natural metal cofactors from enzymes, the functional inhibition of sulfhydryl group-containing proteins or the accelerated formation of reactive oxygen species.[10]

Correlating molecular information on radionuclide speciation and biomolecular interactions with physiological performance is a major challenge for quantitative radioecology. We have recently shown that microcalorimetric monitoring of metabolic activity in combination with genetic engineering can identify molecular details of the modulation of uranium toxicity in a living microorganism.[11] However, the application of microcalorimetry to plant metabolism poses unique challenges. In contrast to bacteria which exhibit exponential growth phases from which division rates can be derived as

physiologically meaningful parameters of toxicity, this is not the case with plant cells. Their metabolism does not follow simple mathematical models and typically declines under the conditions of calorimetric measurements, where photosynthesis is not supported. Whereas non-photosynthetic experimental conditions are compatible with plant cell culture, there is a lack of model-free descriptors that can be used to derive quantitative measures of toxicity from metabolic monitoring. Such descriptors would greatly enhance the value of microcalorimetry in radioecology, because metabolic monitoring has reached a degree of sensitivity that allows detecting actinide toxicity in the environmentally relevant concentrations. Here, lethality is negligible and thus inadequate to derive realistic toxicity measures. In contrast, metabolic responses are clearly visible and render themselves the most sensitive and also biologically most meaningful sensor of toxicity.

In order to overcome these restrictions, we have empirically determined a model-independent descriptor, i.e., “metabolic capacity”, that allows evaluating calorimetric data of declining metabolic phases as typically found with plant cells. In the present work, we used this approach to investigate the concentration-dependent influence of U(VI) on plant cell metabolism using canola callus cells (*Brassica napus*). *B. napus* is known to be able to accumulate heavy metals in higher quantities than many other species.[3] The callus cells are superior over non-callus cells due to their simpler organization and the better control of their growth conditions. At the same time, they retain the ability to synthesize typical secondary metabolites of intact tissues,[12] which renders them a suitable model system for metabolic studies. The “metabolic capacity” of the cells in the presence of 0 to 200 µM U(VI) was determined and correlated with cell viability. We were particularly interested in relating these data to uranium speciation. Therefore, the latter was further assessed by time-resolved laser-induced fluorescence spectroscopy and thermodynamic modeling. Our data

provide both a physiological validation of the descriptor "metabolic capacity" and a speciation-dependent quantification of U(VI) toxicity in a well-established plant cell model.

MATERIALS AND METHODS

Cell Cultivation. Callus cells from *B. napus* (PC-1113) were obtained from DSMZ (Braunschweig, Germany). Friable cells were transferred to liquid modified Linsmaier and Skoog medium (medium R^{13}) to initiate growth of suspension cell cultures on an orbital shaker at room temperature. After a 7 days growth cycle the cells were subcultured into fresh culture medium to maintain the suspension culture. Cell cultures from passage number 2 – 11 were used for microcalorimetry and viability measurements.

Microcalorimetry. Cell suspensions (20 mL) were filtered through a nylon mesh (50 µm pore size) without suction. Subsequently, the cells were rinsed with 10 mL medium R with a reduced phosphate concentration of 12.5 µM representing 1% of the original phosphate concentration (medium R_{red}; pH 5.8; Table S1, supporting information) in order to minimize precipitation of U(VI) phosphate complexes in experiments with uranium. Isothermal calorimetric measurements were performed with a TAM III (Thermal Activity Monitor) instrument (Waters GmbH, Eschborn, Germany) equipped with 12 microcalorimeters in twin configuration (one side for the sample the other for an aluminium reference). Sample preparation time was kept as short as possible. Wet cells (0.3 g) were transferred into 4 mL ampoules with 2 mL of medium R_{red}. A U(VI) stock solution was prepared by dissolution of $UO_2(NO_3)_2 \times 6\ H_2O$ in Milli-Q water (Milli-RO/Milli-Q-System, Millipore, Molsheim, France) and subsequent filtration through 0.2 µm filters (Filtropur S, Sarstedt, Nümbrecht, Germany). The final concentration was 9.58 mM $UO_2(NO_3)_2$ as determined by inductively coupled plasma-mass spectrometry (ICP-MS; model ELAN 9000, Perkin Elmer, Boston, USA).

Aliquots of this stock solution were added to the cell suspensions giving final concentrations of 20-200 µM U(VI). The ampoules were tightly capped, including control samples of medium R_{red} and of cells in medium R_{red} in the absence of U(VI). The samples were held in the TAM III in a waiting position for 15 min before complete insertion followed by 45 min equilibration. In each experiment, thermograms were recorded at least in duplicates in the absence and in the presence of different U(VI) concentrations. Seven independent microcalorimetric experiments with different cell passages were evaluated (details are given in Fig. 2). Over the course of the experiments (up to 300 hours), the pH stayed between 5.5 and 5.9.

Viability Measurements. Cell viability was measured by the MTT test.[14] It detects the activity of mitochondrial and cytosolic dehydrogenases which reduce water-soluble 3-(4,5-dimethylthiazol-2-yl)-2,5-diphenyl-tetrazolium bromide (MTT; Duchefa, Harlem, The Netherlands) to the water-insoluble formazan product accompanied by a yellow to blue color change.[15] A stock solution of MTT (5 mg/mL) was prepared in phosphate buffered saline (PBS, without Ca^{2+} and Mg^{2+}; Biochrom, Berlin, Germany) and passed through a 0.2 µm filter (Filtropur S). At the end of calorimetric data acquisition, the pH values of the nutrient media were measured within the ampoules (inoLab pH meter pH720 and SenTix Mic pH electrode, WTW, Weilheim, Germany). Subsequently, the supernatant medium was removed and the cells were washed twice with 1 mL PBS solution followed by the addition of 1 mL PBS and 200 µL MTT stock solution to each sample. The ampoules were sealed and incubated in the dark under gentle agitation for 3 hours at room temperature. The supernatants were removed and 1 mL 0.04 M HCl (p.a., Merck Darmstadt, Germany) in isopropanol (p.a., Roth, Karlsruhe, Germany) was added to each cell sample to dissolve the formazan crystals. After slight agitation for 10 min at room temperature, 8 × 100 µL of each

isopropanol solution was pipetted into 96-well plates (CELLSTAR®, Greiner Bio-one, Frickenhausen, Germany) and the absorbance at 620 nm determined in a microplate reader (Mithras LB940, Berthold, Bad Wildbad, Germany). Viability of U(VI)-exposed cells was expressed as the absorbance in percent of that from non-exposed control samples. The results represent mean values and standard errors of the mean of a total of 12-24 independent samples.

Time-Resolved Laser-Induced Fluorescence Measurements. Time-resolved laser-induced fluorescence (TRLFS) measurements were performed under ambient conditions at room temperature in order to characterize the U(VI) speciation in medium R_{red}. Aliquots of the 9.58 mM $UO_2(NO_3)_2$ stock solution were added to medium R_{red} to give final concentrations of 20-200 µM U(VI). The pH values of these solutions were readjusted to pH 5.8 with diluted NaOH (Merck) solutions, if necessary. TRLFS studies were performed using a Nd:YAG pumped OPO system (New-Port Spectra Physics, Quanta Ray, USA) with a repetition rate of 20 Hz and laser energies of about 4.4 mJ.[9] The excitation wavelength was 440 nm. Emission signals were focused on the entrance slit of a 270 mm spectrograph (SP2300, Acton Research, Roper Scientific, Martinsried, Germany) and the luminescence spectra detected with an intensified camera system (PIMAX3, Princeton Instruments, Roper Scientific). Using the internal delay generator, time-resolved spectra were recorded during a gate width of 500 ns. In 101 delay steps the gate was shifted to delay times of 0.5 or 5 µs with a step size of 5 or 50 ns, respectively. At each delay time, spectra were recorded with 100 laser pulses per spectrum in the wavelength range between 450.4 and 727.0 nm at a resolution of 0.266 nm. The start wavelength of about 450 nm was selected to avoid scattered light from the exciting laser pulse on the camera. The emission spectra were recorded with WinSpec32

(Roper Scientific), converted into ASCII files and evaluated with the OriginPro 2015G software (OriginLab Corporation, Northampton, USA).

RESULTS AND DISCUSSION

Isothermal Microcalorimetry. We have used heterotrophically growing *B. napus* cells as a model system to investigate interference of U(VI) with plant metabolism. Figure 1 (A and B) shows an example of two unprocessed thermograms obtained from two independent cell cultures in the presence of three different concentrations of U(VI) nitrate.

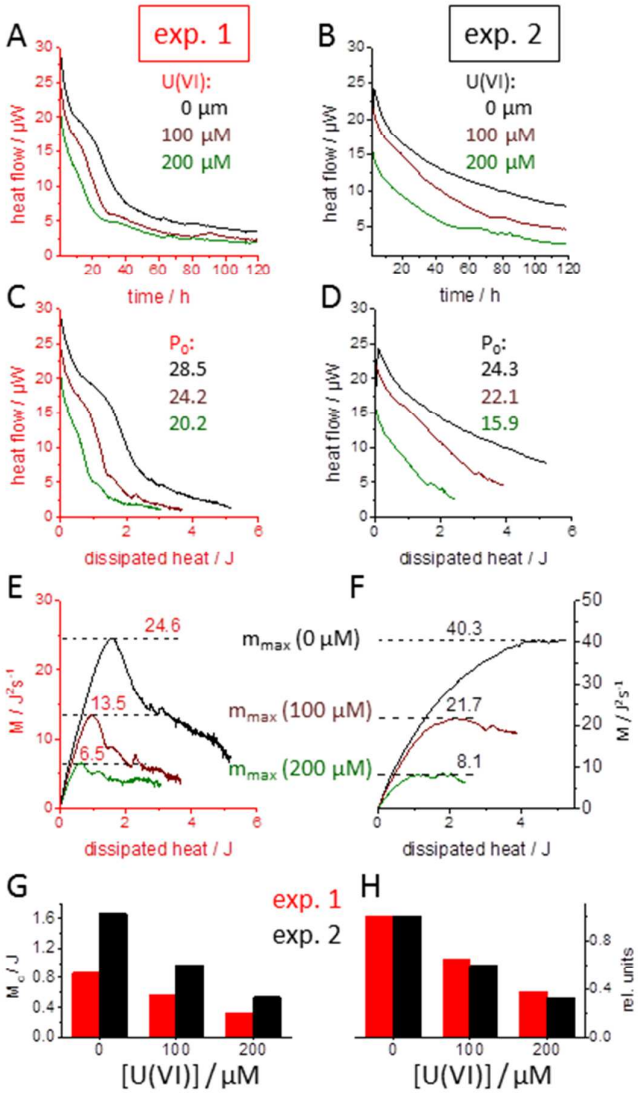

Figure 1: U(VI) dependence of the "metabolic capacity" for distinctly different temporal declines of metabolic activity. Thermograms from two independent *B. napus* cell cultures (left and right panels in A to F) were recorded at 0, 100 and 200 µM U(VI) (raw data in A and B), transformed into enthalpy plots (C and D) and the "metabolic capacity" M calculated (in J^2s^{-1}, E and F). G) The "characteristic metabolic capacity" M_c (in J) was obtained by dividing the M_{max} values by the initial thermal power P_0 of each thermogram (indicated in C and D). H) For comparison, the M_c values from panel G were scaled to unity with respect to the values obtained in the absence of U(VI).

All traces show a temporal decrease in metabolic thermal power and a general reduction of heat production with increasing U(VI) concentration. Despite these robust general trends, the shape of the metabolic decline was biphasic in one case (Fig. 1 A) and resembled an exponential decay in the other (Fig. 1 B). Variability in the thermograms corresponding to cells from different passages was generally observed but typically less than in the depicted examples, where the standard deviation between thermograms (scaled to unity at time zero) was 27%. Consequently, there is no obvious time point at which the comparison of heat flow data would result in an unambiguous ranking of metabolic activity in dependence of U(VI) concentration. Since enzyme activity and substrate supply are the salient determinants of metabolic activity, we have searched for a quantitative descriptor related to these two parameters in order to compare metabolic states.

Whereas enzyme activity generates thermal power (µW), the overall substrate depletion is related to the total dissipated heat (J), because the latter is produced from substrate consumption. We define the "metabolic capacity" M as the product of the time-dependent heat flow P (overall "enzyme activity") and the integrated dissipated heat H (overall "substrate depletion") relative to a time zero (t_0):

$$M(t) := P(t) \cdot H(t), \quad \text{with} \quad H(t) = \int_{t0}^{t} P(t)dt. \qquad (1)$$

M(H) can be calculated from an "enthalpy plot", i.e., the plot of $\frac{dH}{dt}$ (= P) as a function of H (Fig. 1 C and D), by multiplication of each original data pair. The result is graphically displayed for the two independent experiments in Figs. 1 E and F. Since $H(t_0)$ and $P(t\infty)$ are zero, there will always be a characteristic time t_c and enthalpy $H_c = H(t_c)$ at which M(H) reaches a maximum M_{max} in units of J^2s^{-1}. Despite the differently shaped original thermograms, the decrease of M_{max} with increasing U(VI) toxicity was surprisingly similar for the two experiments. Finally, the M_{max} values were normalized with respect to the initial

heat flow P_0 (= $P(t_0)$) of each trace (Fig. 1 C and D), resulting in the "characteristic metabolic capacity" M_c which carries the unit Joule (Fig. 1 G). The virtually identical U(VI) sensitivity of the cells in the two experiments is best appreciated when the M_c values are further scaled to those measured in the absence of uranium (Fig. 1 H). Whereas the raw data show the metabolic activity at a given time point, the derivation of M_c contains the full history of the thermogram up to the time t_c at which M_{max} was reached. The integrative evaluation of thermograms according to Eq. 1 markedly reduced the variation in the M_c values between the two experiments as compared to their original P(t) values at any given time and U(VI) concentration. Importantly, M_c is unambiguously defined and thus independent of subjective choices of data points or physiological models for quantitating toxicity on the basis of metabolic activity. The high reproducibility of the U(VI) sensitivity expressed by M_c values derived from the differently shaped thermograms was surprising. In order to address the physiological relevance of the purely phenomenologically derived value M_c, we analyzed the calorimetric data from seven independent cell cultures (from which 37 thermograms were evaluated) and asked whether the M_c values correlated with representative enzyme activities which are typically used as markers for cell viability and are routinely measured by an MTT test of oxidoreductase activity.[14] The latter was performed either directly after the calorimetric recordings, i. e., at low residual metabolic activity after M_c had been surpassed, or in cell cultures outside the calorimeter under otherwise identical conditions. Calorimetric and enzymatic data were averaged among the studied cultures.

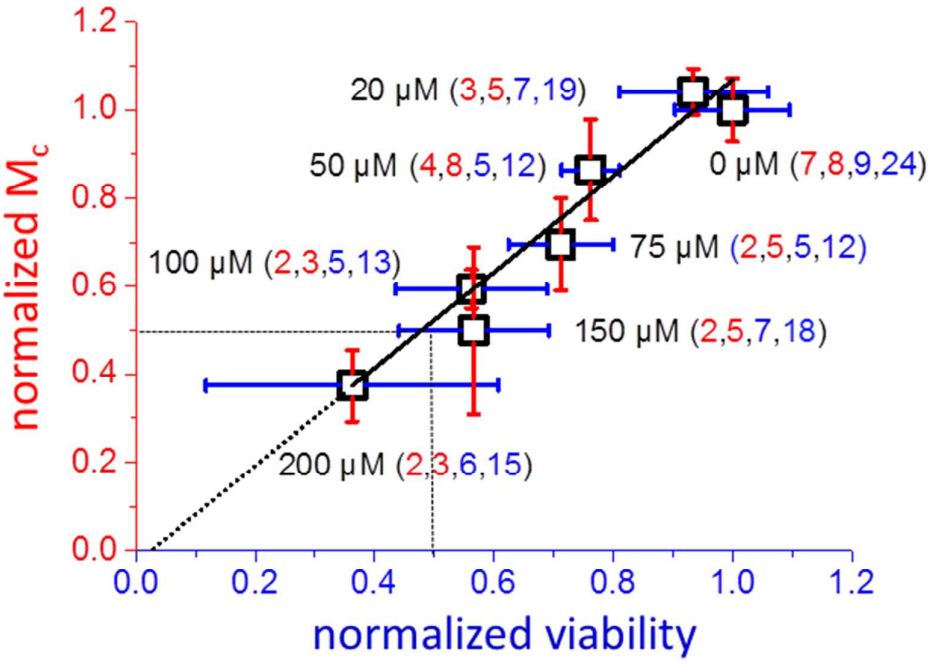

Figure 2: Correlation of oxidoreductase activity (viability) with "characteristic metabolic capacity" M_c. Data were averaged from experiments carried out with several cell cultures (Fig S3). The first and second number in brackets indicates how many cell cultures and thermograms contributed to each microcalorimetric data point, respectively. The third and fourth number give the corresponding information on cell cultures and individual MTT tests. For both assays, the data were normalized to the respective average of the values obtained with control samples in the absence of U(VI). Solid line: linear regression (slope of 1.09 / standard deviation 0.087; intercept -0.02 / standard deviation 0.065; Pearson's R = 0.98). The average standard deviation in the calorimetric (red error bars) and oxidoreductase data (blue error bars) is 15.4 % and 21.9 %, respectively. Dotted lines: projection of half maximal inhibition on the regression line corresponds to an IC_{50} of ~160 µM U(VI).

Figure 2 shows that oxidoreductase activity and M_c are to a very good approximation linearly related at U(VI) concentrations up to 200 µM. The evaluation clearly supports the physiological relevance of the definition of M_c. Therefore, we suggest the use of the "characteristic metabolic capacity" M_c as a calorimetric descriptor of metabolic activities under conditions, where metabolism does not follow simple growth models but declines continuously and with varying time dependence. In the case of *B. napus* cell culture, the M_c

values reveal a half-maximal inhibitory concentration of 160 µM U(VI) which agrees with the MTT viability test due to the almost ideal correlation. The variance in the calorimetric data is smaller and derived from integration over data interval of typically hours, as compared to the MTT test which captures oxidoreductase activity at a subjectively chosen time point. However, the data set is still too small to claim statistical significance (e.g. by a Students t-test).

Calculation of the U(VI) Speciation. The effects of U(VI) on the cell metabolism may depend on its speciation in the medium, i.e., its complexation with biomolecules, organic and inorganic anions. The speciation is known to change with concentration, culture medium composition, and pH value. Therefore, it was further analyzed under the conditions of the calorimetric experiments (supporting information). Table 1 summarizes the main U(VI) species in the medium R_{red} at pH 5.8 at different U(VI) concentrations (sample 1-6). Their pH dependence is shown in Fig. S1.

Under the experimental conditions, the solid UO_2HPO_4 phase dominates at 20 µM $U(VI)_{tot}$ followed by a significant amount of $(UO_2)_3(OH)_5^+$. The latter increases with $U(VI)_{tot}$ and is the dominating species already at $U(VI)_{tot}$ > 50 µM. Besides that, $(UO_2)_4(OH)_7^+$, UO_2OH^+, UO_2^{2+}, and $(UO_2)_2(CO_3)(OH)_3^-$ species are formed, whereas the absolute amount of UO_2HPO_4 (s) remains constant due to the limited phosphate concentration in medium R_{red}.

The calculations included only a single solid U(VI) phase. The significant formation of other phases, i.e., metaschoepite or becquerelite, would be possible, however, can be neglected under the applied conditions. All U(VI) solutions with medium R_{red} were treated by ultracentrifugation (1 hours, 280,000 × g). Due to the ultracentrifugation, a decrease of the U(VI) concentrations in the solutions was observed (see Table S2 supporting information), which can be attributed to the sedimentation of UO_2HPO_4(s). This decrease is higher than

presumed assuming only the formation of UO_2HPO_4(s), however, lower than expected for the additional formation of significant amounts of metaschoepite and becquerelite (see Supporting Information). Thus, we assign the insoluble fraction of U(VI) mainly to UO_2HPO_4(s) and only small amounts of secondary mineral phases and / or U(VI) in colloids formed with nutrient components.

Table 1: Calculated U(VI) speciation in medium R_{red} with solid phases restricted to UO_2HPO_4 (s) only (pH = 5.8, $pCO_2 = 10^{-3.5}$ atm). Species that do not exceed 4% of the total U(VI) concentration ($U(VI)_{tot}$) at any of the analyzed $U(VI)_{tot}$ values are not shown (see Supporting Information for further details).

Sample	$U(VI)_{tot}$ (mol/L)	$(UO_2)_2(CO_3)(OH)_3^-$	$(UO_2)_3(OH)_5^+$	$(UO_2)_4(OH)_7^+$	UO_2OH^+	UO_2^{2+}	UO_2HPO_4(s)
		U(VI) (%)					
1	2.0×10^{-5}	3.66	17.20	1.41	6.10	4.34	62.50
2	5.0×10^{-5}	5.42	49.00	7.70	4.70	3.34	25.00
3	7.5×10^{-5}	5.21	56.80	10.71	3.76	2.68	16.67
4	1.0×10^{-4}	4.94	60.50	12.80	3.18	2.26	12.50
5	1.5×10^{-4}	4.48	63.87	15.80	2.47	1.75	8.33
6	2.0×10^{-4}	4.13	65.50	17.90	2.05	1.46	6.25

Experimental Analysis of U(VI) Speciation. TRLFS measurements were carried out in medium R_{red}. Figure 3(A) shows the time-resolved luminescence spectrum at 50 µM U(VI) and the corresponding decay curve. The latter required bi-exponential approximation, indicating the presence of at least two luminescent species.

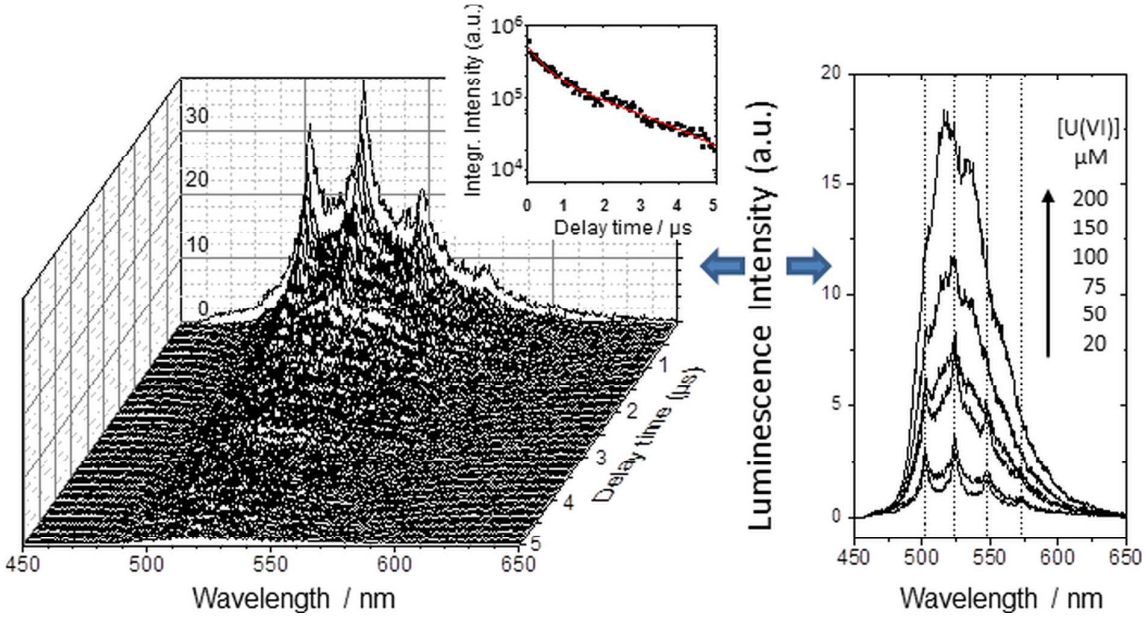

Figure 3: Time-resolved laser fluorescence spectroscopy. A) Spectral dependence of the time-resolved decay of the luminescence of 50 µM U(VI) in medium R_{red} (pH = 5.8) and the decay curve of the integral luminescence intensity (inset). B) Luminescence spectra of U(VI) in medium R_{red} as a function of the total U(VI) concentration (delay time: 51 ns). The vertical lines indicate the peak positions of the initial phosphate species.

Due to the presence of high amounts of organic substances as well as Fe^{3+} and Cl^- (cf. Table S1, supporting information), dynamic quenching processes decreased the luminescence lifetimes, thereby, hampering comparisons with model compounds. Therefore, only the spectral shapes but not the lifetimes were further analyzed. Figure 3 (B) shows U(VI) luminescence spectra recorded at a delay time of 51 ns at different concentrations of $U(VI)_{tot}$. With increasing $U(VI)_{tot}$, the spectra changed significantly indicating a change of the predominant U(VI) solution species. To attribute the spectra to U(VI) species, spectra at different delay times were analyzed by peak deconvolution using the peak fitting module of OriginPro 2015G and compared to literature data (Table S3, supporting information).

The concentration-dependent U(VI) spectra measured after 51 ns (Fig. 3B) lead to specific peak maxima obtained after spectral peak deconvolution. Whereas the peak maxima in samples 1, 5, and 6 stayed constant with increasing delay times, the peaks in samples 2 and 3 showed a progressive hypsochromic shift over time, indicating the predominance of different U(VI) species at different delay times (Figure S2, supporting information). The occurrence of at least two luminescent solution U(VI) species was already concluded from the rough lifetime estimation. The comparison of the peak maxima with those of reference species (Table S3, supporting information) shows that U(VI) phosphate species dominated in sample 1 and contributed also to the luminescence of sample 2-4 at 51 ns. At longer delay times, the spectra corresponded to $(UO_2)_3(OH)_5^+$ which was also the case for sample 5 and 6. For the latter, the constancy of the spectra over all delay times demonstrated the dominance of this species at $U(VI)_{tot}$ > 100 µM. Although the luminescence lifetimes of all samples were generally strongly quenched, a shorter lifetime of the U(VI) phosphate species was observed than for the U(VI) hydroxo species (not shown). This agrees with literature data, where luminescence lifetimes of 6.0 µs and 4.7 ± 0.1 µs were reported for UO_2HPO_4 and $(UO_2)_x(PO_4)_y$, respectively[16] in contrast to 19.8 ± 1.8 µs for $(UO_2)_3(OH)_5^+$.[17] The TRLFS results are further supported by the thermodynamic speciation calculations: UO_2HPO_4 and $(UO_2)_3(OH)_5^+$ dominates the U(VI) speciation at 20 µM and ≥ 50 µM $U(VI)_{tot}$, respectively (cf. Table 1).

U(VI) Speciation and Metabolic Activity. Microcalorimetry has been used previously for the assessment of U(VI)-dependent bacterial activities both in genetically engineered bacteria[11] or communities found in uranium waste heaps.[18] Typically, calorimetric studies have been evaluated based on mathematically well-defined growth models [19] or enthalpy balances[20] in order to derive per cell estimates of metabolic rates. However, metabolic

calorimetry suffers from the lack of quantitative descriptors when simple growth models cannot be applied. This is particularly the case with plant cells in the presence of heavy metals which exhibit metabolic decline rather than growth. On the other hand, calorimetry is particularly attractive for assessing radionuclide toxicity in the environmentally relevant low dose exposure. Calorimetry is non-invasive, toxicity estimates can be derived directly from the physical response of a living system, and experimental procedures enable minimal handling efforts with radionuclides. In order to exploit the potential of microcalorimetry in radioecological investigations, we have established a generally applicable evaluation of thermograms from cells that exhibit metabolic decline without a preceding growth phase. We have shown here that the "characteristic metabolic capacity" M_c (Eq. 1) is a reliable calorimetric descriptor that scales with enzymatically determined viability in *B. napus* cells. Using this descriptor, the influence of U(VI) speciation on metabolic activity can be addressed. The TRLFS data and the thermodynamic modeling showed that the total amount of U(VI) hydroxo complexes in fresh medium R_{red} increased with $U(VI)_{tot}$, whereas the low phosphate concentration in medium R_{red} limited $UO_2HPO_4(s)$ formation to less than 13 µM. Figure 4 correlates M_c with $U(VI)_{tot}$ and, alternatively, with the sum of the two hydroxo complexes that make up more than 50% of all species for $[U(VI)_{tot}] > 20$ µM (Table 1). The normalized M_c values scale linearly with the U(VI) hydroxo complexes. Importantly, the data intersect the y-axis nearly perfectly at the expected value of $M_c = 1$ for [U(VI) hydroxo complexes] = 0. Although M_c varies linearly also with $[U(VI)_{tot}] > 0$, the required condition of $M_c = 1$ for $[U(VI)_{tot}] = 0$ is not met. The data indicate that the dissolved hydroxo-species possess highest bioavailability. In contrast, species that are not bioavailable ($UO_2HPO_4(s)$) contribute to $U(VI)_{tot}$ without lowering M_c. This explains the right-shift of the plot of M_c *vs.* $U(VI)_{tot}$. Correspondingly, metabolism is suppressed by 50% at a concentration of ~ 90 µM of

304 the U(VI) hydroxo-complexes (intersection of regression line with x-axis, Fig. 4) which is
305 significantly less than the ca. 160 µM estimated from the regression line in Fig. 2, where the
306 indicated $[U(VI)]_{tot}$ concentration includes also non-bioavailable U(VI) species.

307 Speciation-dependence of U(VI) uptake and translocation is a general phenomenon. Both
308 are affected by pH in *Arabidopsis thaliana* plants, although pH also altered the cellular redox
309 balance in this organism.[5] In contrast to the majority of invasive biochemical studies on U(VI)
310 uptake and toxicity, isothermal microcalorimetry can provide a highly sensitive and non-
311 invasive monitor of radionuclide-mediated metabolic effects. We have shown here for *B.*
312 *napus* cells that metabolic responses of plant cells to U(VI) can be measured under the non-

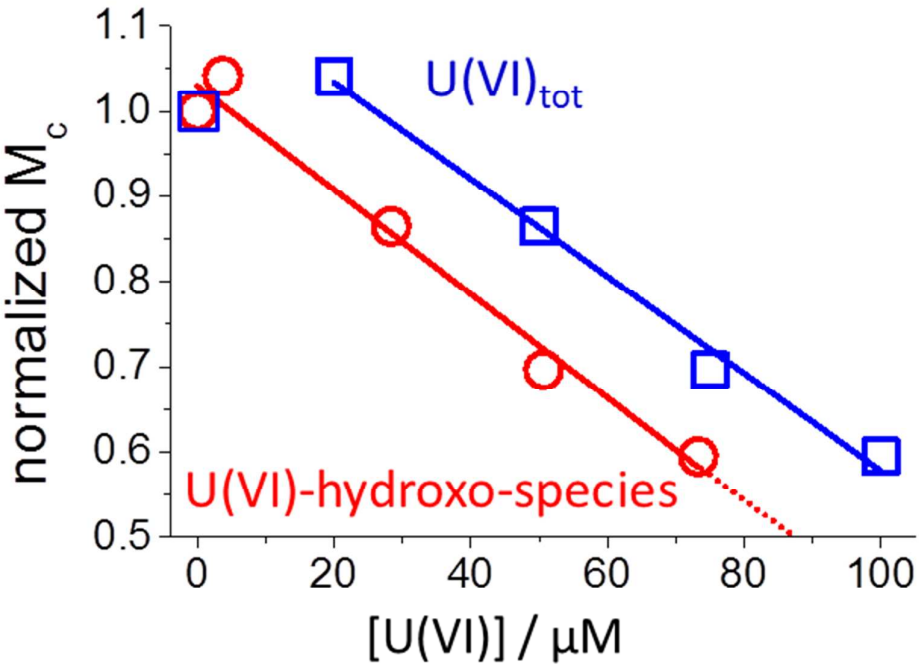

Figure 4: U(VI) species-dependency of the "characteristic metabolic capacity" M_c. Circles: the normalized M_c values (from Fig. 2) are plotted *vs.* the concentration of the dominant hydroxo-species, i.e., $[(UO_2)_3(OH)_5^+] + [(UO_2)_4(OH)_7^+]$. Squares: the same M_c values plotted *vs.* $U(VI)_{tot}$. Solid lines: linear regression of the data. The strong correlation (Pearson's R = 0.99) of M_c with the U(VI)-hydroxo-species (red) indicates that it is biologically the most relevant (dotted line: extrapolation to IC_{50} of ~90 µM).

313 photosynthetic regime of microcalorimetry. Remarkably, the "characteristic metabolic
314 capacity" M_c correlates sufficiently well with an established enzymatic viability test to be
315 used as a quantitative descriptor of toxicity. It appears less variable than the enzymatic test,
316 which is probably due to the integration of thermal data over time as opposed to the single
317 time point estimates obtained by the MTT test. The current observation is statistically not
318 significant (by Student's t-test) but a systematic comparison of error margins in M_c
319 determinations and enzymatic assays will be interesting once larger data sets are available.
320 The current study demonstrates the potential of life cell microcalorimetry for radioecological
321 studies, enabling viability measurements independently of prior genetic or detailed
322 physiologic analyses. At the same time, handling of radionuclides can be reduced to an
323 absolute minimum. Although microcalorimetry has been shown to also reveal mechanistic
324 details on uranium toxicity when linked to genetic engineering[11], such data complement but
325 cannot replace studies on uranium-dependent specific enzyme activities (for example
326 Saenen at el. 2015). Instead, the strength of life cell microcalorimetry originates in its quick
327 and non-invasive systemic approach. It appears particularly suited for the future
328 quantification of toxicity mediated by internal exposure to other α- and β-emitting uranium
329 isotopes for which the present work provides the necessary reference. It remains to be
330 elucidated to which extend such investigations can contribute to the ecotoxicological risk
331 assessment of radionuclides, where endpoints at higher degrees of biological complexity
332 such as metabolism-driven processes (growth and development) may provide the missing
333 link to the effects of radionuclides at the molecular scale[21].
334

ACKNOWLEDGEMENTS

The authors thank Dr. M. H. Obeid, J. Seibt, S. Heller, and J. Philipp for their valuable help with the performance of the experiments, S. Gurlitt and B. Pfützner for ICP-MS measurements, and S. Weiss for ultracentrifugation.

Associated Content

SUPPORTING INFORMATION

Thermodynamic Modeling of the U(VI) Speciation in Medium R_{red}

Table S1, S2, Fig. S1

Analysis of TRLFS Data

Table S3, Fig S2

Dose response curves of metabolic capacity and oxidoreductase activity

Fig. S3

References

1. Ebbs, S. D.; Brady, J.; Kochian, L. V. Role of uranium speciation in the uptake and translocation of uranium by plants. *J. Exp. Bot.* **1998,** *49*, 1183-1190.
2. Laurette, J.; Larue, C.; Mariet, C.; Brisset, F.; Khodja, H.; Bourguignon, J.; Carrière, M. Influence of uranium speciation on its accumulation and translocation in three plant species: Oilseed rape, sunflower and wheat. *Environ. Exp. Bot.* **2012,** *77*, 96-107.
3. Laurette, J.; Larue, C.; Llorens, I.; Jaillard, D.; Jouneau, P.-H.; Bourguignon, J.; Carrière, M. Speciation of uranium in plants upon root accumulation and root-to-shoot translocation: A XAS and TEM study. *Environ. Exp. Bot.* **2012,** *77*, 87-95.
4. Misson, J.; Henner, P.; Morello, M.; Floriani, M.; Wu, T.-D.; Guerquin-Kern, J.-L.; Février, L. Use of phosphate to avoid uranium toxicity in *Arabidopsis thaliana* leads to alterations of morphological and physiological responses regulated by phosphate availability. *Environ. Exp. Bot.* **2009,** *67*, 353-362.
5. Saenen, E.; Horemans, N.; Vanhoudt, N.; Vandenhove, H.; Biermans, G.; Van Hees, M.; Wannijn, J.; Vangronsveld, J.; Cuypers, A. Effects of pH on uranium uptake and oxidative stress responses induced in *Arabidopsis thaliana*. *Environ. Toxicol. Chem.* **2013,** *32*, 2125-2133.
6. Saenen, E.; Horemans, N.; Vanhoudt, N.; Vandenhove, H.; Biermans, G.; van Hees, M.; Wannijn, J.; Vangronsveld, J.; Cuypers, A. Oxidative stress responses induced by uranium exposure at low pH in leaves of *Arabidopsis thaliana* plants. *J. Environ. Radioact.* **2015,** *150*, 36-43.
7. Viehweger, K.; Geipel, G.; Bernhard, G. Impact of uranium(U) on the cellular gluthathione pool and resultant consequences for the redox status of U. *Biometals* **2011,** *24*, 1197-1204.
8. Günther, A.; Bernhard, G.; Geipel, G.; Reich, T.; Roßberg, A.; Nitsche, H. Uranium speciation in plants. *Radiochim. Acta* **2003,** *91*, 319-328.
9. Geipel, G.; Viehweger, K. Speciation of uranium in compartments of living cells. *Biometals* **2015,** *28*, 529-539.
10. Weiler, E.; Nover, L. *Allgemeine und molekulare Botanik;* Georg Thieme Verlag: Stuttgart, 2008; p 900.
11. Obeid, M. H.; Oertel, J.; Solioz, M.; Fahmy, K. Mechanism of attenuation of uranyl toxicity by glutathione in *Lactococcus lactis*. *Appl. Environ. Microbiol.* **2016,** *82*, 3563-3571.
12. Zagoskina, N. V.; Goncharuk, E. A.; Alyavina, A. K. Effect of cadmium on the phenolic compounds formation in the callus cultures derived from various organs of the tea plant. *Russ. J. Plant Physiol.* **2007,** *54*, (2), 237-243.
13. Linsmaier, E. M.; Skoog, F. Organic Growth Factor Requirements of Tobacco Tissue Cultures. *Physiol. Plantarum* **1965,** *18*, 100-127.
14. Mosmann, T. Rapid colorimetric assay for cellular growth and survival: application to proliferation and cytotoxicity assays. *J. Immunol. Methods* **1983,** *65*, 55-63.
15. Lindl, T.; Gstraunthaler, G. *Zell- und Gewebekultur;* 6 ed.; Spektrum Akademischer Verlag: Heidelberg, 2008.
16. Billard, I.; Geipel, G. Luminescence Analysis of Actinides: Instrumentation, Applications, Quantification, Future Trends, and Quality Assurance. *Springer Ser. Fluoresc.* **2008,** *5*, 465-492.
17. Sachs, S., Brendler, V., Geipel, G. Uranium(VI) complexation by humic acid under neutral pH conditions studied by laser-induced fluorescence spectroscopy. *Radiochim. Acta* **2007,** *95*, 103-110.
18. Schippers, A.; Hallmann, R.; Wentzien, S.; Sand, W. Microbial Diversity in Uranium-Mine Waste Heaps. *Appl. Environ. Microbiol.* **1995,** *61*, 2930-2935.
19. Braissant, O.; Bonkat, G.; Wirz, D.; Bachmann, A. Microbial growth and isothermal microcalorimetry: Growth models and their application to microcalorimetric data. *Thermochim. Acta* **2013,** *555*, 64-71.
20. Maskow, T.; Paufler, S. What does calorimetry and thermodynamics of living cells tell us? *Methods* **2015,** *76*, 3-10.
21. Fuller, N.; Lerebours, A.; Smith, J.T.; Ford, A.T. The biological effects of ionising radiation on Crustaceans: A review. *Aquat. Toxicol.* **2015,** *167,* 55-67.

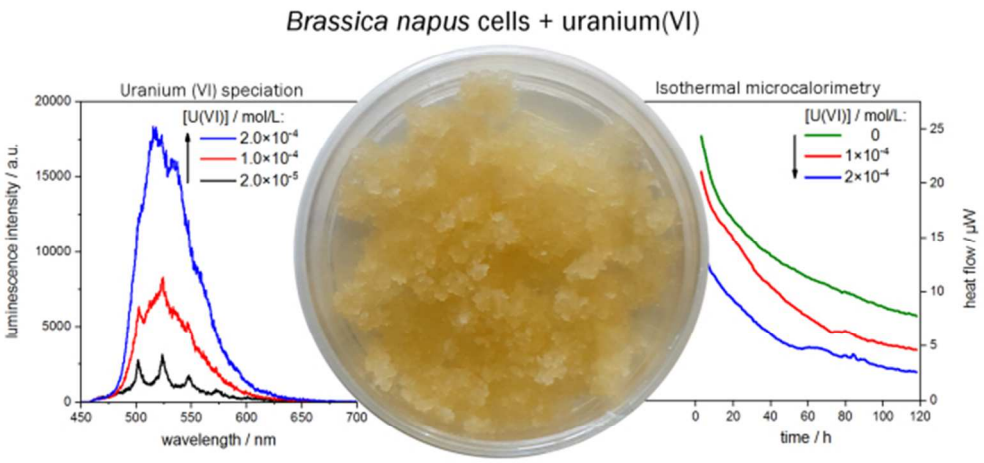

TOC graphical abstract

84x47mm (200 x 200 DPI)